

# Multispectral optical imaging device for *in vivo* detection of oral neoplasia

**Darren Roblyer**  
**Rebecca Richards-Kortum**

Rice University  
Department of Bioengineering  
6100 Main St.  
Houston, Texas 77251-1892  
E-mail: dmr2@rice.edu

**Konstantin Sokolov**

University of Texas M. D. Anderson Cancer Center  
Departments of Imaging Physics and Biomedical  
Engineering  
1515 Holcombe Boulevard  
Houston, Texas 77030

**Adel K. El-Naggar**  
**Michelle D. Williams**

University of Texas M. D. Anderson Cancer Center  
Department of Pathology  
1515 Holcombe Blvd., Box 0085  
Houston, Texas 77030

**Cristina Kurachi**  
**Ann M. Gillenwater**

University of Texas M.D. Anderson Cancer Center  
Department of Head and Neck Surgery  
1515 Holcombe Boulevard, Unit 441  
Houston, Texas 77030

## 1 Introduction

Oral cancer poses a significant world health problem, ranking as the sixth most common cancer globally,<sup>1</sup> causing over 127,000 deaths worldwide each year.<sup>2</sup> In the United States alone, there were<sup>3</sup> an estimated 30,990 cases of oral cancer diagnosed and 7430 deaths in 2006. Oral cancer often goes undiagnosed until the later stages of development, resulting in high mortality. In the United States, the 5-yr survival rate for localized oral cancer is 81%, but this drops to only 30% for advanced disease,<sup>4</sup> suggesting that early detection has the ability to save many lives. In addition, patients who survive an initial occurrence of oral cancer are known to be at an increased risk of developing a second malignancy, highlighting the importance of continued surveillance of this population.<sup>5</sup>

The most common screening method for oral cancer is visual inspection and palpation of the mouth. Physicians inspect for clinically evident oral lesions such as leukoplakia (white patches) or erythroplakia (red patches), which are associated with increased risk of oral cancer.<sup>1,6</sup> Visual examination relies heavily on the experience and skill of the physician

**Abstract.** A multispectral digital microscope (MDM) is designed and constructed as a tool to improve detection of oral neoplasia. The MDM acquires *in vivo* images of oral tissue in fluorescence, narrow-band (NB) reflectance, and orthogonal polarized reflectance (OPR) modes, to enable evaluation of lesions that may not exhibit high contrast under standard white light illumination. The device rapidly captures image sequences so that the diagnostic value of each modality can be qualitatively and quantitatively evaluated alone and in combination. As part of a pilot clinical trial, images are acquired from normal volunteers and patients with precancerous and cancerous lesions. In normal subjects, the visibility of vasculature can be enhanced by tuning the reflectance illumination wavelength and polarization. In patients with histologically confirmed neoplasia, we observe decreased blue/green autofluorescence and increased red autofluorescence in lesions, and increased visibility of vasculature using NB and OPR imaging. The perceived lesion borders change with imaging modality, suggesting that multimodal imaging has the potential to provide additional diagnostic information not available using standard white light illumination or by using a single imaging mode alone.

© 2008 Society of Photo-Optical Instrumentation Engineers. [DOI: 10.1117/1.2904658]

**Keywords:** oral cancer; diagnosis; noninvasive; optical imaging; fluorescence; decreased autofluorescence; reflectance; polarized; orthogonal; porphyrin; vasculature; monochromatic.

Paper 07279R received Jul. 26, 2007; revised manuscript received Nov. 19, 2007; accepted for publication Dec. 10, 2007; published online May 1, 2008.

to identify and delineate early premalignant and cancerous changes. Several benign conditions, such as lichen planus, inflammation, and hyperkeratosis, mimic the clinical presentation of precancerous lesions, and visual inspection with standard white light illumination may not yield sufficient contrast between normal and abnormal tissues. Once a suspicious lesion is identified, biopsy and histological examination are required for definitive diagnosis. Biopsies are invasive, painful, and costly and require familiarity and skill and are therefore typically limited to highly suspicious lesions. Additionally, many lesions are heterogeneous in morphology and visual appearance, and biopsy diagnosis may not be representative of the entire lesion due to the small sampling area.<sup>7</sup> Approaches that can help differentiate between normal and neoplastic areas and that can reduce the need for evaluator experience have the potential to greatly facilitate and improve early diagnosis of oral cancer.

Optical imaging has the potential to address these clinical challenges. The contrast between normal and neoplastic areas can be increased beyond that which is available with standard white light by tuning illumination and detection conditions. Reflectance imaging can detect local changes in scattering and absorption of tissue, and fluorescence imaging can probe changes in the biochemical composition of tissue by revealing

Address all correspondence to Rebecca Richards-Kortum, Department of Bioengineering, Rice University, 6100 Main Street, Houston, TX 77005, USA; Tel: 713-348-5869; Fax: 713-348-5877; E-mail: rkortum@rice.edu

levels of endogenous fluorophores. These changes have shown to be indicative of malignant progression<sup>8</sup> and are targeted in a variety of imaging modalities to detect and diagnose premalignant changes in different anatomic sites including the cervix,<sup>9</sup> gastrointestinal tract,<sup>10</sup> lung,<sup>11</sup> and oral mucosa.<sup>6,8,12–17</sup> High-resolution optical imaging techniques such as confocal microscopy and optical coherence tomography have the potential to image changes in tissue architecture and cellular morphology. A drawback to *in vivo* cellular resolution microscopy however, is the small field of view (FOV) interrogated, making screening of an entire mucosal surface impractical without an initial means of guidance toward suspicious areas. Wide-field optical imaging techniques enable clinicians to screen several centimeters at a time for identification of margins and optimal sites for further interrogation by small-FOV imaging techniques or biopsy.

Several wide-field optical imaging systems have shown promise in improving detection of neoplastic lesions in the oral and oropharyngeal regions. Lane et al. presented a non-magnifying hand-held device for direct visualization of oral cavity tissue fluorescence.<sup>6</sup> The system uses a metal-halide lamp with emission peaks at 405 and 436 nm to excite tissue autofluorescence. Images obtained using this device showed a characteristic decrease of green fluorescence associated with oral precancer and cancer. Decreased green fluorescence distinguished normal tissue from severe dysplasia, carcinoma *in situ*, or invasive carcinoma in 50 biopsy sites from 44 patients with a sensitivity of 98% and specificity of 100%, using histology as the gold standard. This device is available commercially as the VELscope<sup>®</sup>, which is Food and Drug Administration (FDA) approved and is currently in clinical use. De Veld et al. provide an excellent review of the status of *in vivo* autofluorescence imaging for oral oncology.<sup>8</sup>

While fluorescence imaging alone has shown great promise for detection of neoplastic lesions in the oral cavity, incorporating additional imaging techniques may increase the effectiveness and sensitivity of wide-field optical devices. Techniques that are capable of detecting increases in vascular density and changes in light scattering properties may be particularly useful, since these features have previously been associated with the development of cancer, and are not easily detected by fluorescence imaging alone.<sup>18</sup> Additionally, reflectance imaging systems tend to be simpler in design compared to fluorescence devices, thereby reducing instrument complexity and cost. In narrow-band (NB) reflectance imaging, tissue is illuminated using a 10 to 20 nm wavelength band and reflected light is imaged. The optical contrast of microvasculature close to the epithelial surface can be increased by selecting an illumination band that matches peaks in the absorption spectrum of hemoglobin.<sup>19</sup> Another approach to increase contrast is to control the polarization of the illumination source and detected light. In orthogonal polarization reflectance (OPR) imaging, tissue is illuminated with linearly polarized light; a second linear polarizer is placed in front of the detector and oriented so that only reemitted light with a polarization orthogonal to the illumination is captured. This has the effect of selectively detecting photons that have undergone multiple scattering events in the tissue (resulting in a reduction in degree of polarization) and rejecting those singly scattered photons returning from the surface of the tissue. This technique enables observation of deeper or birefringent

tissue structures and enhances the prominence of microvasculature due to increased hemoglobin absorption.<sup>20</sup> When both orthogonal and parallel polarization images are captured, they can be mathematically combined to form a composite image, which has been shown useful for imaging skin pathologies.<sup>20</sup> Lindeboom et al. described orthogonal polarization spectral (OPS) imaging of oral tumor sites using a magnifying hand-held device coupled to a CCD camera, designed to provide maximum contrast between the microvasculature and surrounding tissue.<sup>21</sup>

The multispectral digital microscope (MDM) was developed to investigate the diagnostic effectiveness of combining multiple imaging modalities in a single device. The MDM acquires high-resolution, wide-field images *in vivo*, using white light illumination, fluorescence excitation, NB, and OPR modes. It employs a wide range of illumination wavelengths to investigate which provide the greatest contrast between normal and neoplastic areas for each imaging mode. In this paper, we describe the design of the device, evaluate its optical performance, and present sample images obtained in human subjects with the MDM system.

## 2 Materials and Methods

### 2.1 Instrumentation

Figure 1 shows an optical schematic of the MDM. The OPMI<sup>®</sup> picodental microscope (Carl Zeiss, Jena, Germany) is used as the core optical component of the MDM. The magnification setting is adjusted by turning a lens turret to one of five positions. Light is routed from the source to the microscope head by a fiber optic light guide. The working distance of the microscope is 25 cm. The FOV of the device is dependent on the choice of magnification setting and ranges between 1 and 4 cm in diameter. With a monitor size of 17 in., the system magnification ranges from 8.5 times to 34.7 times.

The original light source was replaced with an air-cooled 100-W mercury arc lamp (Photon Technology International, Birmingham, New Jersey), housed in a custom light box. The lamp and ellipsoidal reflector produce a converging beam which is collimated using a 25-mm planoconvex lens (Lambda Optics, Costa Mesa, California). To protect both the patient and optical components from excessive heating, a cold mirror (Barr Associates, Westford, Massachusetts) is used to eliminate unwanted IR radiation, and an absorbing glass filter removes UV light at wavelengths below 350 nm. The beam then passes through a 10-position excitation filter wheel (Sutter Instruments, Novato, California) and through a second planoconvex lens, which focuses the beam onto the proximal face of a 5-mm-diam fused quartz light guide (Fiberoptic Systems, Simi Valley, California), which routes the light to the microscope head. Since the microscope was not originally designed to support near-UV excitation, a custom-machined adaptor was implemented to bypass the original illumination optics and to hold the distal end of the light guide and a fused quartz focusing lens (Newport Optics, Stratford, Connecticut). This adaptor provides a significant increase in near-UV excitation power and subsequently reduces exposure times required for fluorescence imaging. The adaptor also holds a linear polarizer (Chroma Technologies, Rockingham, Vermont), which is servo controlled and engaged by the LabVIEW (Austin, Texas) interface.

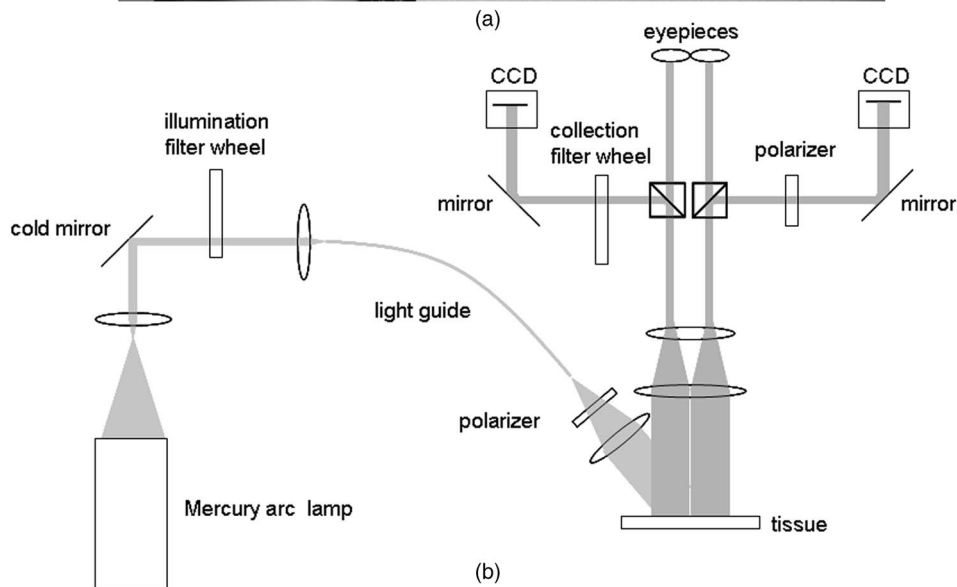


Fig. 1 (a) MDM in the Head and Neck Clinic at the MD Anderson Cancer Center and (b) system optical schematic.

The illumination filter wheel contains narrow-band illumination filters at 420, 430, 530, and 600 nm for NB imaging. These wavelengths were selected to match hemoglobin absorption features, and also to provide multiple wavelengths throughout the visible spectrum to study the effects of wavelength on penetration depth. The illumination filter wheel also contains illumination filters centered at 365, 380, 405, and 450 nm for autofluorescence excitation. These excitation wavelengths were chosen based on previous work by Heintzelman et al.<sup>13</sup> and Utzinger et al.<sup>22</sup> The full width at half maximum (FWHM) transmission bandwidth for the excitation filters ranges from 20 nm for NB imaging to 50 nm for UV illumination (Chroma Technologies, Omega Optics). A 1.0 neutral density filter is used to attenuate the white light illumination power. A light-blocking disk occupies one position in the excitation filter wheel and is used for measurement of the background light level.

The emission arm of the MDM consists of a Zeiss objective lens and 50/25/25 beamsplitter, which passes 50% of the emission light to the microscope eyepieces and 25% each to two CCD detectors. An emission filter wheel (Oriol Optics, Stratford, Connecticut) is located in one detection arm and contains long-pass filters and a linear polarizer. A long-pass filter with a cut-on at 410 nm is used with the 365- and 380-nm excitation, one with a cut-on at 430 nm is used with 405-nm excitation wavelength, and one with a cut-on at 475 nm is used with 450-nm excitation. An additional linear polarizer is placed in the opposing detector arm, as shown in Fig. 1. In one arm, the polarizer is oriented parallel to the excitation polarizer and in the other, the polarizer is oriented perpendicular to the excitation polarizer. The opposing polarizers enable simultaneous OPR and parallel polarization imaging; this feature is useful for reducing changes in FOV that can occur due to patient movement.

**Table 1** Irradiance and typical exposure times for each illumination condition.

Illumination, $\lambda$ (nm)	Imaging Modality	Irradiance (mW/cm <sup>2</sup> )	Typical Exposure (ms)
365	fluor.	11.15	100
380	fluor.	8.86	160
405	fluor.	7.00	400
450	fluor.	5.10	500
white	reflect	12.02	16
420	reflect	3.13	64
430	reflect	9.62	13
530	reflect	1.91	24
600	reflect	4.17	64
white, polarized	polarized	11.15	100

Two Retiga Exi (QImaging, Burnaby, BC, Canada) 12-bit color-cooled cameras are used to collect image data. This camera model was chosen because of its low-light sensitivity and compatibility with the LabVIEW programming environment. The sensor is a Sony ExHAD ICX285 progressive-scan high-sensitivity CCD chip, providing adequate spectral sensitivity at chosen wavelengths of interest, from 400 to 650 nm. The chip is covered by a Bayer Mask mosaic for color imaging. Image data are saved in raw Bayer format and color interpolation is performed in postprocessing based on color-balancing standards.

Control of the MDM system is accomplished by a custom LabVIEW graphical interface. The interface provides the operator with the ability to image with one excitation/emission wavelength pair at a time, or to collect a rapid sequence of image data over the range of the MDM's capabilities. The interface also enables the user to store information such as study number and patient data, which are linked and saved with the optical data. Imaging parameters are recorded for all data collected, and background measurements are taken with each sequence.

The MDM takes about 1 min to collect a complete image sequence. The sequence is composed of white light reflectance, fluorescence, NB, OPR, parallel polarization reflectance, and background data sets. A predefined set of exposure and gain settings was established for each image in the sequence based on measurements of normal volunteers. To account for interpatient variability, measurement site variability, and changes due to disease, the predefined set of exposure times could be manually scaled up or down in 20% intervals during imaging. Additionally, four duplicate images were taken for each illumination/emission setting at lower and higher exposure times relative to the initial choice. Table 1 shows typical exposure times based on the most commonly used exposure settings used in the pilot clinical trial.

A set of standards was chosen to quantify the performance of the MDM as well as to track any changes occurring in the device over time. Positive reflectance standards include 99, 75, and 50% reflectance spectralon disks (Labsphere, North Sutton, New Hampshire), and red, green, and blue portions of a Macbeth Color Chart (GretaMacbeth LLC, New Windsor, New York). A 2% spectralon disk serves as a negative reflectance standard. Positive fluorescence standards include a set of four fluorescent slides (Microscopy/Microscopy Education, microscopyeducation.com) and the negative fluorescence standard is a frosted quartz disk (Mark Optics, Santa Ana, California).

For white light illumination, color balance was achieved by imaging a white balance sheet and adjusting the RGB ratio in software so that equal pixel intensity values were obtained in the red, green, and blue channels. For fluorescence imaging, a constant color balance was used throughout the study to maximize qualitative diagnostic ability and to reflect the natural blue-green tissue fluorescence color. The fluorescence color slides were used as a standard to track any changes in color response of the camera over time in fluorescence mode.

## 2.2 Pilot Clinical Study

Several sites within the oral cavity of normal subjects were imaged using the MDM as part of an Institutional Review Board (IRB)-approved protocol at Rice University. In a separate, ongoing pilot clinical study conducted at the University of Texas M. D. Anderson Cancer Center (MDACC), the MDM was used to image clinically abnormal and normal oral mucosal sites in patients. This protocol was approved by the IRBs at both Rice University and MDACC.

The measurements were performed either in the outpatient clinic or in the operating room on patients under general anesthesia prior to surgery. The areas to be imaged were chosen by the clinician and included areas that had previously been identified as abnormal by clinical examination and/or biopsy. The physician first evaluated these targeted areas using the MDM under white light illumination, adjusting the focus and FOV. Several measurement sequences were then taken from each subject including abnormal sites, and when possible, a corresponding contralateral normal site. Excess saliva was suctioned prior to imaging. Because teeth exhibit particularly strong autofluorescence, attempts were made to cover any teeth in the FOV with low-fluorescence gloves or a mouth guard. The head of the patient was positioned and held by the physician during imaging to reduce motion artifacts. In patients seen in the clinic, biopsies were obtained from clinically abnormal sites and a contralateral normal site. In patients who underwent surgical excision, the resected specimens were histologically examined. A clinical diagnosis for normal and abnormal-appearing areas (graded as normal, abnormal but not suspicious for neoplasia, suspicious for neoplasia, or cancer) was rendered by the clinician. The histopathology diagnosis of biopsy sites and resected tissue from imaged areas were considered the gold standard for diagnosis.

Four observers (DR, CK, AG, RRK) examined the images to identify features that differed in abnormal sites compared to clinically normal areas, and which might be further explored for diagnostic relevance. Qualitative observations of image data were correlated with clinical observations regarding pe-

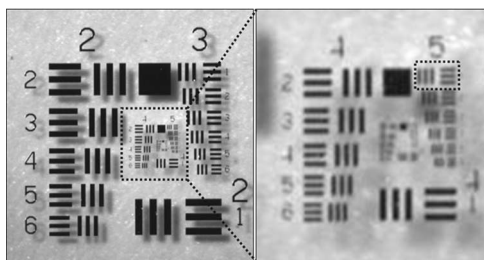


**Fig. 2** USAF resolution target imaged at high magnification. Element 5 group line spacings of  $15.6 \mu\text{m}$  (shown in the dashed box) are easily discriminated in the zoomed-in image on the right.

ripheral extent of abnormal changes and clinical diagnostic category. Pathology results from resected tissue and biopsies enabled comparison between MDM image data and histopathologic diagnosis of lesions.

### 3 Results

#### 3.1 Instrument Performance

The resolution of the MDM was determined by imaging a U.S. Air Force (USAF) spatial resolution target, as shown in Fig. 2. A line spacing of  $15.6 \mu\text{m}$  (group 5, element 1) can clearly be discriminated at the highest magnification. The appearance of shadowing behind each element is due to the finite thickness of the glass substrate, and is not intrinsic to the MDM system. Measurements of white light illumination on a 99% reflectance spectralon standard (Labsphere, North Sutton, New Hampshire) show a 4-cm-diam illumination spot size. This is adequate to illuminate all but the edges of the FOV at the most commonly used magnification. The illumination pattern is Gaussian due to light guide coupling.

To confirm the absence of excitation filter leakage and adequacy of performance of longpass filters, a 2-in.-diam frosted quartz disk was imaged in fluorescence mode. Exposure times and gain settings matching or exceeding those used for normal tissue fluorescence imaging were used at each excitation/emission wavelength pair to confirm the absence of signal from the nonfluorescent frosted quartz disk. The ratio of autofluorescence signal from tissue to frosted quartz was always greater than 10:1.

Intrasequence image registration was affected by patient movement, generally causing some changes in the FOV during the course of the image sequence. Figure 4 (in Sec. 3.3) shows several images taken from a typical sequence in a clinical setting at the most common magnification setting. Using user-defined selection of points common to both images, the linear translation was less than 60 pixels (less than 5% of the FOV) between any two of the images in the sequence in both the  $x$  and  $y$  directions.

UV radiation during all human measurements is well below the American Conference of Governmental Industrial Hygienists maximum allowed rating.<sup>23</sup>

#### 3.2 MDM Images of Normal Oral Sites

Sites imaged in the oral cavity from four normal volunteers included tongue, buccal, lip, gingiva, hard palate, soft palate, and floor of mouth. Fine vasculature was clearly identifiable in images acquired from the lip, floor of mouth, hard palate,

and soft palate using white light, NB, OPR and fluorescence techniques. These images serve as further examples of the resolution capabilities of the MDM. Figure 3 shows an image of the lower lip of a normal volunteer under several illumination conditions. The white light image [Fig. 3(A)] shows microvasculature from a variety of depths beneath the epithelial surface. The OPR image illustrates similar vascular patterns; specular reflection is no longer visible in the image, and spatial resolution is somewhat reduced because the OPR technique selectively records photons that have undergone more scattering events in the tissue. The NB image obtained with 420-nm illumination [Fig. 3(B)] shows only the superficial, fine vasculature due to the reduced penetration of this wavelength; vessel contrast is also increased because this wavelength matches the Soret absorption band of hemoglobin. As the illumination wavelength is increased from green [Fig. 3(D)] to red [Fig. 3(F)], vessels deeper within the tissue are visible in the image. The NB image obtained with 600-nm illumination shows a loss of contrast and spatial resolution due to the increased ratio of scattering to absorption and increased mean free path between scattering events at this wavelength. Vasculature was not as apparent in the buccal and tongue.

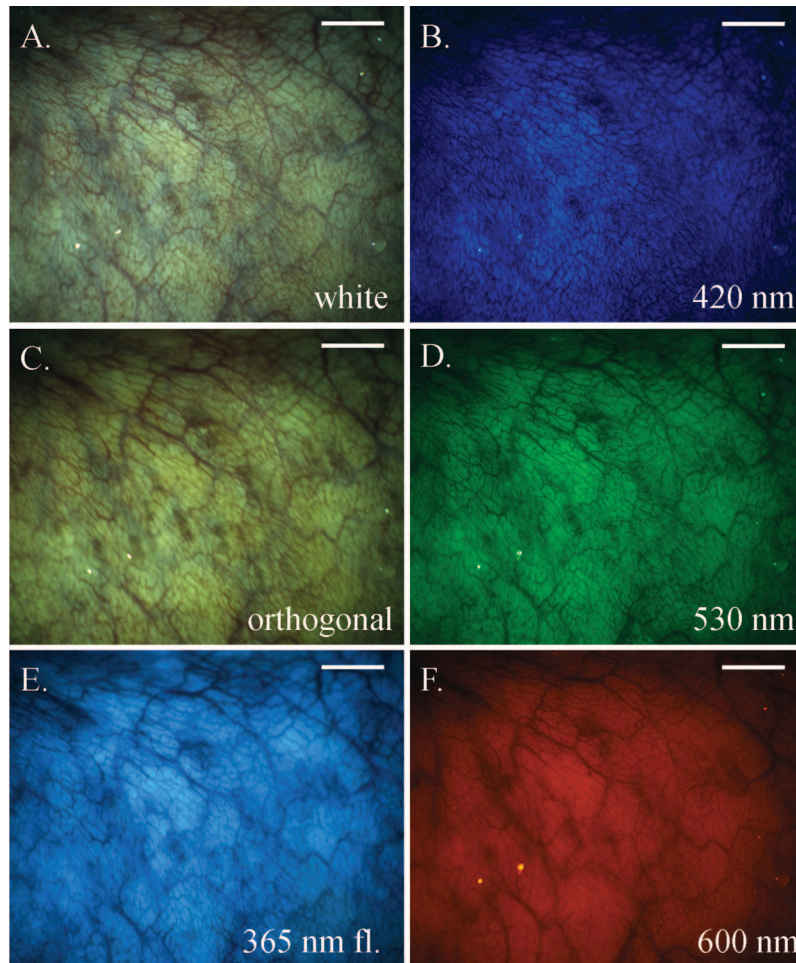
Tissue autofluorescence is predominantly blue at UV excitation wavelengths [Fig. 3(E)] and blue-green at the longer 450 nm excitation. The hard palate, soft palate, floor of mouth, and buccal mucosa provided a higher fluorescence signal than the tongue, gingiva, and lip. The midline of the hard palate was particularly bright. Teeth were highly fluorescent and tooth fluorescence could be seen through portions of the gingival mucosa. Blood vessels appeared dark under fluorescence mode compared to the surrounding tissue. Red fluorescence occasionally appeared on the dorsal tongue.

#### 3.3 MDM Images of Oral Dysplasia and Cancer

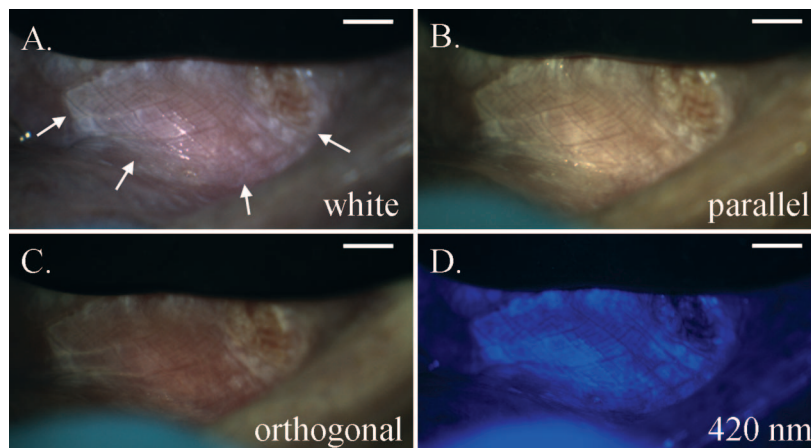
Images of a premalignant lesion and an invasive cancer are presented as representative examples to demonstrate the capabilities of the MDM system for examination of the oral cavity. Some images were cropped to only show relevant areas.

Figure 4 shows images obtained from a thin leukoplakia lesion (indicated by arrows) on the right mandibular gingiva. The thin leukoplakia in the OPR image [Fig. 4(C)] is less evident demonstrating the ability of OPR imaging to selectively detect photons that have scattered more deeply into the tissue. The blue NB image [Fig. 4(D)] shows the leukoplakia as brighter in reference to surrounding tissue compared to the white light image.

Figure 5 shows images acquired from a subtle lesion on the right lateral tongue. The clinical impression of the lesion was leukoplakia, but not overly suspicious for dysplasia or cancer. Following imaging, a  $2.4 \times 1.0 \times 0.4 \text{ cm}^3$  volume was surgically resected and histopathology showed moderate squamous dysplasia [Fig. 5(H)]. The standard white light image [Fig. 5(A)] shows some patchy irregularities in the mucosal surface. Using the green NB [Fig. 5(E)] and the OPR imaging conditions [Fig. 5(C)], an apparent increase in visual contrast was observed between the lesion and surrounding normal areas (indicated by arrows in each case). A decreased blue/green autofluorescence (DA) was observed in the area of the lesion in fluorescence images at 365-, 380-, and 405-nm



**Fig. 3** Images of normal volunteer inner lip: (A) white light illumination image, (B) 420-nm NB image, (C) OPR image, (D) 530-nm NB image, (E) 365-nm excited fluorescence image, and (F) 600-nm NB image. Note increased contrast of vasculature in (C) compared to white light image. Fine vasculature is visible in (B), whereas deep, larger diameter vasculature is visible in (F). Scale bars indicate 0.3 cm.



**Fig. 4** Images of leukoplakia lesion on right gingiva: (A) white light illumination image, arrows indicate area of leukoplakia; (B) parallel polarization image; (C) OPR image; and (D) 420-nm NB image. Note that the OPR (C) enables visualization of tissue below the thin leukoplakia and the 420-nm OPR image (D) accentuates areas of leukoplakia. Scale bars indicate 0.25 cm.

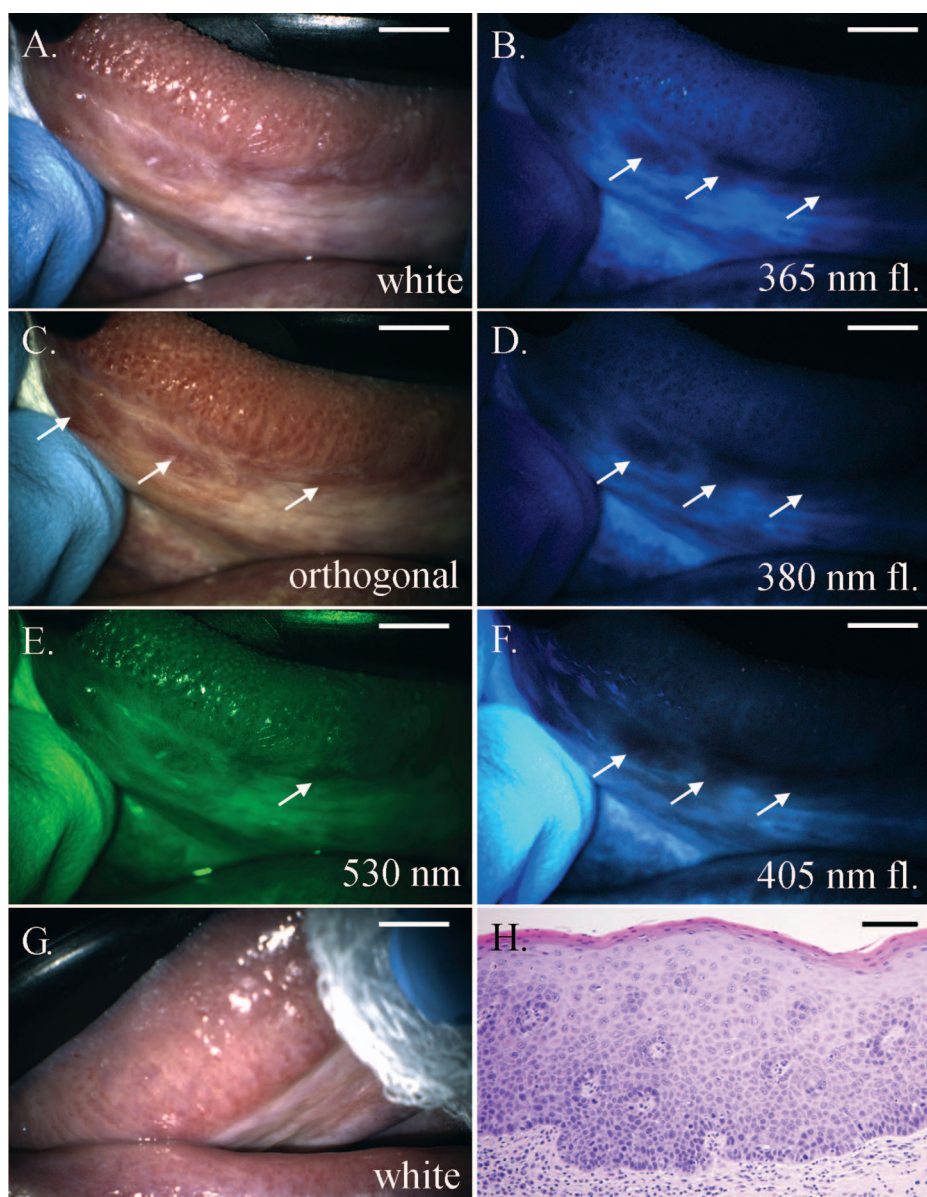


**Fig. 5** Images from tongue of patient with leukoplakia, (A) to (F) show a FOV containing areas along the lateral aspect of the tongue, which were resected and found to contain moderate dysplasia: (A) white light illumination image, (B) 356-nm excited fluorescence image, (C) OPR image, (D) 380-nm excited fluorescence image, (E) 530-nm NB image, (F) 405-nm excited fluorescence image, (G) white light illumination image of contralateral normal site, (H) hematoxylin and eosin (H&E)-stained tissue from abnormal area indicating moderate dysplasia. Arrows indicate areas with loss of fluorescence or increased contrast. Scale bars indicate 0.5 cm in (A) to (G) and 200  $\mu\text{m}$  in (H).

excitation [Figs. 5(B), 5(D), and 5(F)]. An image of a contralateral normal area imaged using white light is shown in Fig. 5(G) for comparison.

Figure 6 shows images acquired from a premalignant lesion on the left lateral tongue. The clinical impression was erythroplakia; a reddish lesion associated with a high risk of dysplasia or early carcinoma. Histopathology from a biopsy of the lesion indicated severe squamous dysplasia with a focal ulceration and chronic inflammation [Fig. 6(H)]. Both the OPR image [Fig. 6(C)] and the green NB image [Fig. 6(E)] showed an area of abnormality (appearing darker red on OPR and darker on NB images as indicated by arrows), which is more extensive in peripheral extent and has increased contrast as viewed against the surrounding mucosa. In the images ob-

tained using all four fluorescence excitation wavelengths a comparative decrease or loss of blue or green fluorescence was seen in the abnormal site. The total area of DA was larger at 405-nm excitation [Fig. 6(F)] than at 365-nm [Fig. 6(B)] and 380-nm excitation [Fig. 6(D)]. In addition, a striking ring of increased red fluorescence surrounding the lesion was observed in the fluorescence images, and is most apparent at 405-nm excitation. This red fluorescence is consistent with the presence of endogenous porphyrins. A white light image obtained from a contralateral normal area is shown in Fig. 6(G) for comparison.

Figure 7 shows images from the right lateral tongue in a subject with histologically confirmed carcinoma. A previously biopsied and ulcerative lesion is shown in the center of the

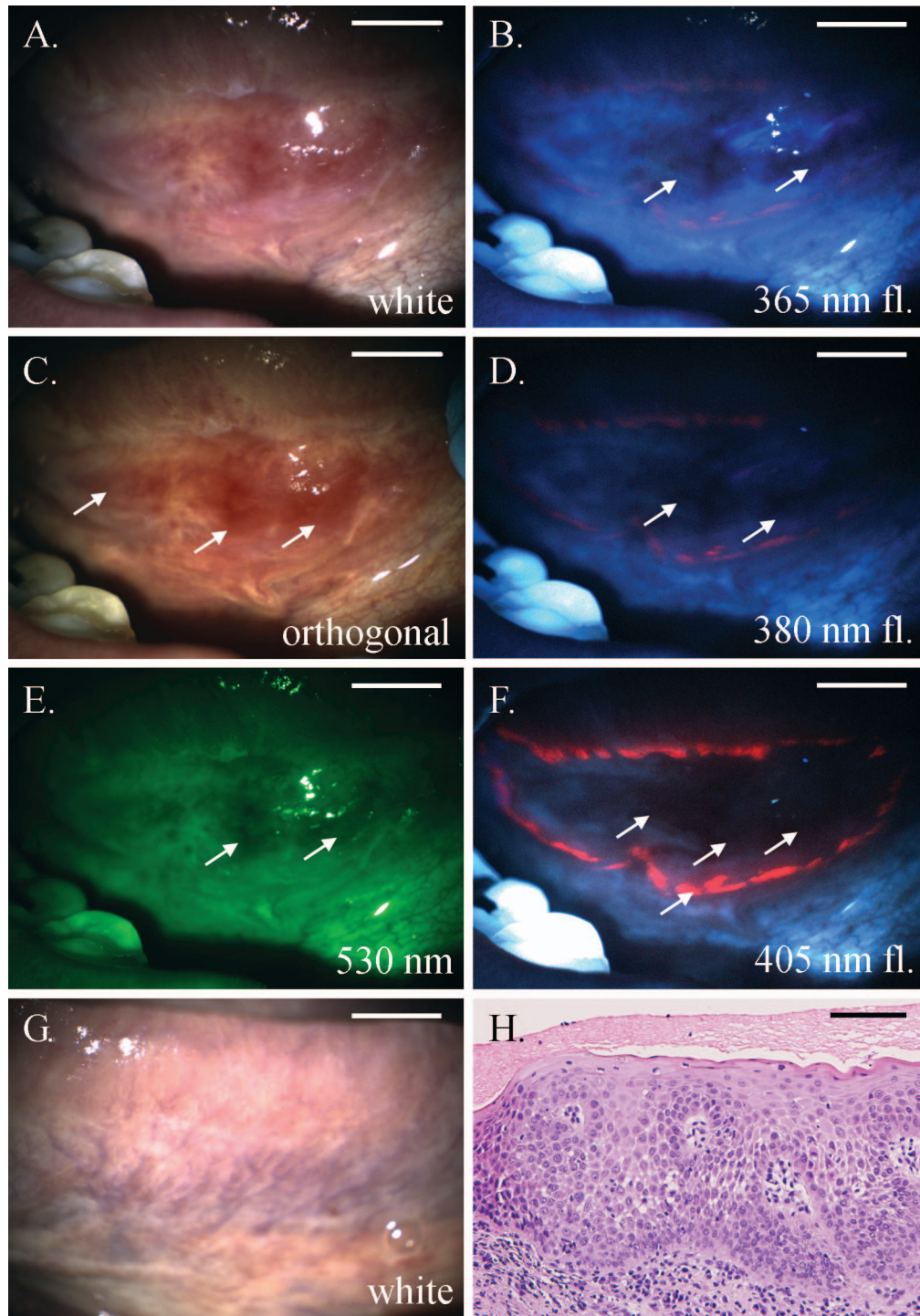


**Fig. 6** Images from ventral tongue of patient with erythroplakia, (A) to (F) show a FOV of the left lateral tongue containing erythroplakia from clinical appearance and severe dysplasia from histopathology of biopsy site: (A) white light illumination image, (B) 356-nm excited fluorescence image, (C) OPR image, (D) 380-nm excited fluorescence image, (E) 530-nm NB image, (F) 405-nm excited fluorescence image, (G) white light illumination image of contralateral normal site, and (H) H&E-stained tissue from abnormal area indicating severe dysplasia. Arrows indicate areas with loss of fluorescence or increased contrast. Scale bars indicate 0.5 cm in (A) to (G) and 200  $\mu\text{m}$  in (H).

FOV. In the OPR image [Fig. 7(B)], the blue NB image [Fig. 7(C)], and the green NB image [Fig. 7(E)], increased contrast is noted by arrows in the tissue surrounding the ulcer. The blue NB image [Fig. 7(C)] shows larger dark areas in the ulcerative lesion and in the bottom right compared to the

white light image [Fig. 7(A)]. The red NB image [Fig. 7(G)] shows smaller dark areas compared to white light. The fluorescence images show a decrease of blue/green fluorescence surrounding the ulcerative lesion, and this DA is more apparent for 405- and 450-nm excitation [Figs. 7(F) and 7(H)] than

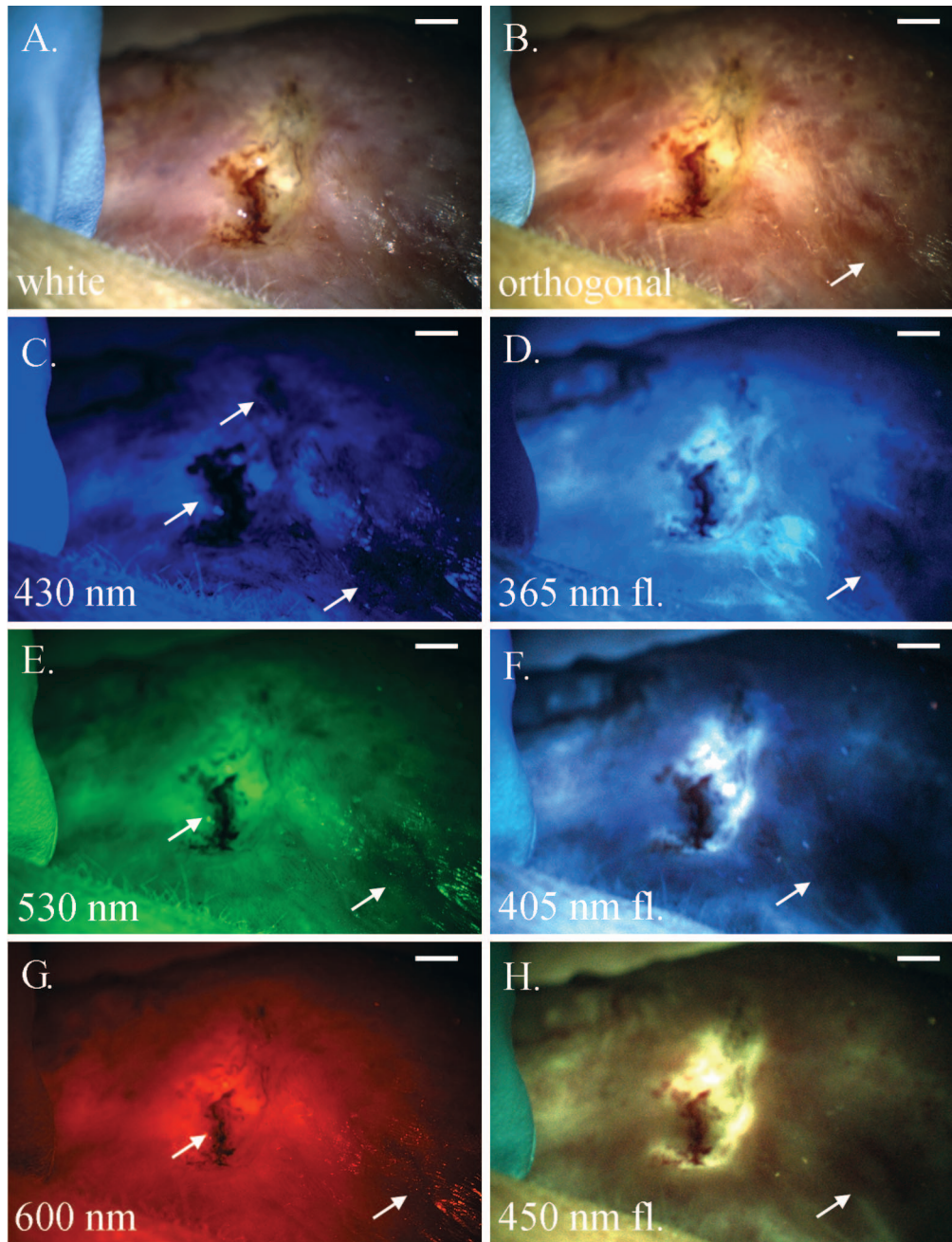


**Fig. 7** Images from cancer on right lateral tongue: (A) white light illumination image, (B) OPR image, (C) 430-nm NB image, (D) 365-nm excited fluorescence image, (E) 530-nm NB image, (F) 405-nm excited fluorescence image, (G) 600-nm NB image, and (H) 450-nm excited fluorescence image. Arrows indicate increased contrast or decreased autofluorescence. Scale bars indicate 0.25 cm.

at 365-nm excitation [Figs. 7(D) and 7(E)]. Following imaging, a  $3.2 \times 2.5 \times 1.0 \text{ cm}^3$  portion was resected and was determined by histopathology to contain invasive squamous carcinoma centrally, with dysplasia near the margins of resection.

In these representative examples, we observe one or more of the following features in areas histologically determined to be abnormal: a decrease of blue/green fluorescence, increased red fluorescence, and an increase of contrast in highly vascular regions. Blood on the surface of the tissue also appeared dark compared to white light under blue and green NB illumination. Teeth and gloves occasionally interfered with fluo-

rescence imaging of tissue due to their autofluorescence, as can be seen in the lower left corner of the fluorescence frames in Fig. 5.

#### 4 Discussion

In this study, DA was observed in many clinically abnormal areas compared to surrounding normal tissue, and this finding was common to all four fluorescence excitation wavelengths. DA was also observed surrounding submucosal, exophytic, or hyperkeratotic abnormal areas as well as in clinical lesions

lacking the white keratotic surface associated with leukoplakia. Areas with DA did not always correspond to areas where increased contrast was seen using other modalities. Increased red fluorescence was observed in about half the patients imaged. It appeared most often on cancerous regions and on necrotic tissue but occasionally appeared in clinically dysplastic or precancerous areas. Red fluorescence did not usually correlate with DA or with increased contrast from NB or OPR imaging.

Blue and green NB images tended to increase contrast of visible blood vessels and areas suspected of containing a high density of superficial microvasculature. Blue illumination revealed fine vasculature, which appeared superficial, whereas illumination at green or red wavelengths revealed larger diameter, deeper vasculature. The 530-nm illumination was most useful in increasing negative contrast in lesions in the study patients. Blood on the surface of the tissue also appeared dark under blue and green NB excitation. OPR had the effect of reducing specular reflection and increasing negative contrast in some abnormal regions compared to imaging under conventional white light illumination. Both OPR and NB appear useful for detecting areas with high microvascular density, and in many cases, the resulting images showed extended margins of clinically abnormal areas compared to white light imaging. In most cases, discrete vessels were observed in normal contralateral measurements and at the periphery of abnormal areas, while diffuse, homogeneous red areas were observed on abnormal lesions with flat contours. Elevated lesions in cancerous or precancerous areas often obscured vascular detail.

The characteristic DA associated with neoplasia has been extensively explored to determine abnormal areas in previous imaging studies in the oral cavity.<sup>6,15,17,24</sup> It has been suggested that a decrease of collagen cross-links and decreased density of matrix fibers is the major contributor to loss of green fluorescence; these are important features that may be associated to malignant progression. Pavlova et al.<sup>25</sup> and Drezek et al. have shown that precancerous cervical tissue exhibits decreased stromal fluorescence due to a decreased density of matrix fibers. Lane et al., who used excitation light from 400 to 460 nm, suggest collagen-related DA as a major mechanism enabling contrast between the appearance of neoplastic areas and normal tissue using<sup>6,26</sup> the Velscope®.

Increased red fluorescence in the oral cavity is well documented for carcinoma, and in previous imaging studies,<sup>12,14,17,27</sup> red fluorescence was best observed when excited at approximately 410 nm. Inaguma and Hashimoto found the presence of red fluorescence in 85% of the 78 lesions of oral carcinomas they investigated.<sup>12</sup> Ingrams et al. obtained 90% sensitivity and 91% specificity for the discrimination of normal and dysplastic/malignant mucosa using the presence of red fluorescence.<sup>28</sup> This red fluorescence is generally attributed to the presence of porphyrins whose origins in biological tissue are disputed. It is unclear whether they are a by-product of abnormal metabolism in tissue or if it is produced by bacteria contaminating the surface of the tissue.

Changes in contrast using NB and OPR have been previously observed in oral tissue and are likely due to increased microvasculature density and structure associated with malignant transformation. Pazouki et al. showed an increase in vascularity in oral tissue throughout malignant progression.<sup>18</sup> By

choosing reflectance excitation wavelengths that correspond to hemoglobin spectral features, the NB reflectance images maximize microvasculature visualization and contrast. Subhash et al. used this technique to detect abnormal tissue in the oral cavity. They showed that the ratio of two oxygenated hemoglobin dips at 540 and 575 nm decreased in excised malignant tissue compared to normal.<sup>19</sup> De Felice et al. speculated that observed optical changes in the color spectrum observed in bronchopulmonary dysplasia may be caused by an altered microvasculature network.<sup>29</sup> Wavelength-dependent photon penetration depth utilized in NB reflectance imaging may also provide useful depth dependent diagnostic information.

OPR techniques enabled us to look deeper into tissue by utilizing the ability to reject singly scattered photons that have retained their polarization state. Photons that have had their polarization state altered either by multiple scattering events or by birefringent properties of the tissue are selectively detected. This can have the effect of providing negative contrast against surrounding tissue when imaging vasculature, and of making vasculature networks lying deep to the surface appear visible. Lindeboom et al.<sup>21</sup> used orthogonal polarization spectral imaging to observe vascular patterns in patients with oral SCC. They found that in 80% of the cases from 10 patients, capillary density was increased in tumorous areas and in 90% of the cases, disarrangement of capillary morphology correlated with tumorous areas.

This pilot trial was designed to demonstrate the capabilities of the MDM as well as to make preliminary qualitative observations of abnormal lesions in humans. Further studies of larger groups of patients are required to determine the utility of each imaging technique compared to white light inspection, as well as to determine which combinations of techniques afford the most useful predictive information. Contributions from inflammation or benign conditions to DA or increased contrast in NB imaging will affect the specificity of detection and it will be important to determine these effects. Additionally, precise pathology correlations will be key to future studies. Correlations in this study were made using histopathologically diagnosed biopsy or resected tissue data that were known to be within the FOV during image collection. Biopsy data provide information on only a small fraction of the imaged FOV and represents a limitation of this pilot study. Improved techniques for spatial correlation between histopathologic sections and image data will be required in future work.

The MDM described here can obtain high-quality images of the oral cavity using multiple imaging modalities. To facilitate comparison between modalities, images were collected in rapid sequences from the same FOV. Pilot clinical data indicate that additional imaging modalities such as NB and OPR may provide information not available in fluorescence mode alone, and may be useful in discriminating precancerous and cancerous tissue from normal and benign or inflammatory regions.

#### Acknowledgments

The authors gratefully acknowledge support from the National Institutes of Health (NIH) Grants No. R21 DE 16485 and No. R01 CA 103830.

## References

1. S. Silverman, "Oral cancer," in *Atlas of Clinical Oncology*, Hamilton, London: American Cancer Society.
2. D. M. Parkin et al., "Global cancer statistics, 2002," *Ca-Cancer J. Clin.* **55**(2), 74–108 (2005).
3. American Cancer Society, *Cancer Facts and Figures: 2005*, American Cancer Society (2005).
4. A. Jemal et al., "Cancer statistics," *Ca-Cancer J. Clin.* **55**(1), 10–30 (2005).
5. H. Shibuya et al., "Multiple primary cancer risk in patients with squamous cell carcinoma of the oral cavity," *Cancer* **60**(12), 3083–3086 (1987).
6. P. M. Lane et al., "Simple device for the direct visualization of oral-cavity tissue fluorescence," *J. Biomed. Opt.* **11**(2), 024006 (2006).
7. D. P. Slaughter, H. W. Southwick, and W. Smejkal, "Field cancerization in oral stratified squamous epithelium; clinical implications of multicentric origin," *Cancer* **6**(5), 963–968 (1953).
8. D. C. De Veld et al., "The status of *in vivo* autofluorescence spectroscopy and imaging for oral oncology," *Oral Oncol.* **41**(2), 117–131 (2005).
9. R. A. Drezek et al., "Optical imaging of the cervix," *Cancer* **98**(Suppl 9), 2015–2027 (2003).
10. H. Zeng and C. MacAulay, "Real-time endoscopic fluorescence imaging for early cancer detection in the gastrointestinal tract," *Bioimaging* **6**, 151–165 (1998).
11. S. Lam, "Localization of bronchial intraepithelial neoplastic lesions by fluorescence bronchoscopy," *Chest* **3**, 696–702 (1998).
12. M. Inaguma and K. Hashimoto, "Porphyrin-like fluorescence in oral cancer: *in vivo* fluorescence spectral characterization of lesions by use of a near-ultraviolet excited autofluorescence diagnosis system and separation of fluorescent extracts by capillary electrophoresis," *Cancer* **86**(11), 2201–2211 (1999).
13. D. L. Heintzelman et al., "Optimal excitation wavelengths for *in vivo* detection of oral neoplasia using fluorescence spectroscopy," *Photochem. Photobiol.* **72**(1), 103–113 (2000).
14. K. Onizawa et al., "Usefulness of fluorescence photography for diagnosis of oral cancer," *Int. J. Oral Maxillofac Surg.* **28**(3), 206–210 (1999).
15. R. Paczona et al., "Autofluorescence videoendoscopy for photodiagnosis of head and neck squamous cell carcinoma," *Eur. Arch. Otorhinolaryngol.* **260**(10), 544–548 (2003).
16. K. Onizawa et al., "Fluorescence photography as a diagnostic method for oral cancer," *Cancer Lett.* **108**(1), 61–66 (1996).
17. B. Kulapaditharom and V. Boonkitticharoen, "Laser-induced fluorescence imaging in localization of head and neck cancers," *Ann. Otol. Rhinol. Laryngol.* **107**(3), 241–246 (1998).
18. S. Pazouki et al., "The association between tumour progression and vascularity in the oral mucosa," *J. Pathol.* **183**(1), 39–43 (1997).
19. N. Subhash et al., "Oral cancer detection using diffuse reflectance spectral ratio R540/R575 of oxygenated hemoglobin bands," *J. Biomed. Opt.* **11**, 014018 (2006).
20. S. L. Jacques, J. C. Ramella-Roman, and K. Lee, "Imaging skin pathology with polarized light," *J. Biomed. Opt.* **7**(3), 329–340 (2002).
21. J. A. Lindeboom, K. R. Mathura, and C. Ince, "Orthogonal polarization spectral (OPS) imaging and topographical characteristics of oral squamous cell carcinoma," *Oral Oncol.* **42**(6), 581–585 (2006).
22. U. Utzinger et al., "Optimal visual perception and detection of oral cavity neoplasia," *IEEE Trans. Biomed. Eng.* **50**(3), 396–399 (2003).
23. ACGIH, *American Conference of Governmental Industrial Hygienists Threshold Limit Values and Biological Exposure Indices for Chemical and Physical Agents*, Signature, Cincinnati, OH (2004).
24. C. S. Betz et al., "A comparative study of normal inspection, autofluorescence and 5-ALA-induced PPIX fluorescence for oral cancer diagnosis," *Int. J. Cancer* **97**(2), 245–252 (2002).
25. I. Pavlova et al., "Microanatomical and biochemical origins of normal and precancerous cervical autofluorescence using laser-scanning fluorescence confocal microscopy," *Photochem. Photobiol.* **77**(5), 550–555 (2003).
26. C. F. Poh et al., "Direct fluorescence visualization of clinically occult high-risk oral premalignant disease using a simple hand-held device," *Head Neck* **29**(1), 71–76 (2007).
27. C. S. Betz et al., "Autofluorescence imaging and spectroscopy of normal and malignant mucosa in patients with head and neck cancer," *Lasers Surg. Med.* **25**(4), 323–334 (1999).
28. D. R. Ingrams et al., "Autofluorescence characteristics of oral mucosa," *Head Neck* **19**(1), 27–32 (1997).
29. C. De Felice et al., "Abnormal oral mucosal light reflectance in bronchopulmonary dysplasia," *Early Hum. Dev.* **82**(4), 273–278 (2006).